

## On the symmetry and crystal chemistry of britholite: New structural and microanalytical data

ROBERTA OBERTI,<sup>1,\*</sup> LUISA OTTOLINI,<sup>1</sup> GIANCARLO DELLA VENTURA,<sup>2</sup> AND GIAN CARLO PARODI<sup>3</sup>

<sup>1</sup>CNR-CS per la Cristallografia e la Cristallografia, via Ferrata 1, I-27100 Pavia, Italy

<sup>2</sup>Dipartimento di Scienze della Terra, Università della Calabria, I-87030 Arcavacata di Rende, Italy

<sup>3</sup>Laboratoire de Minéralogie, Museum National d'Histoire Naturelle, rue Buffon 61, F-75005 Paris, France

### ABSTRACT

We provide in this paper complete structural and micro-chemical characterization of two britholite samples with compositions  $(\text{Mn}_{0.04}\text{Ca}_{4.75}\text{REE}_{4.37}\text{Th}_{0.72}\text{U}_{0.12})\Sigma_{10.00}(\text{Si}_{5.57}\text{P}_{0.25}\text{B}_{0.16})\Sigma_{5.98}\text{O}_{24}(\text{OH}_{0.23}\text{F}_{1.77})\Sigma_{2.00}$  (from Latium, Italy) and  $(\text{Na}_{0.98}\text{Ca}_{2.01}\text{REE}_{6.97})\Sigma_{9.96}(\text{Si}_{5.07}\text{P}_{0.75})\Sigma_{5.82}\text{O}_{24}(\text{OH}_{0.53}\text{F}_{1.47})\Sigma_{2.00}$  (from Los Islands, Guinea). The crystal-chemical formulae were calculated by combining electron-microprobe analyses for intermediate-Z elements (Na, Ca, Mn, Si, P), ion-microprobe analyses for low-Z (H, Li, Be, B, F) and high-Z elements (Ba, Y, REE and actinides), and high-quality ( $R_{\text{obs}}$  1.2–2.6) single-crystal structure refinements. Structure refinements indicate that the best approximation to the real symmetry is the  $P6_3$  space group. In britholite, the lowering of symmetry with respect to the  $P6_3/m$  space group of apatite means that the O3 and O3a atoms are no longer equivalent and allows the tetrahedron to rotate up to  $\sim 4^\circ$  around the Si-O1 bond. Consequently, the O3a atom moves closer to the REE1a site, whereas the O3 atom moves farther from the REE1 site and closer to the REE2 site, which thus assumes a [7+1] coordination. The infrared spectrum of britholite from Latium shows a unique and very broad band in the OH-stretching region at  $3437\text{ cm}^{-1}$ , which is consistent with the ordering of trivalent REE cations at the REE2 site. The calculated integral molar absorptivity  $\epsilon_i$  is  $23600\text{ L}\cdot\text{mol}^{-1}\cdot\text{cm}^{-2}$ . A remarkable constancy in the unit-cell volume along the whole apatite-britholite compositional range is observed for values of the aggregate ionic radius at the REE sites shorter than  $1.12\text{ \AA}$  and longer than  $1.15\text{ \AA}$ , whereas large variations are observed for intermediate values; this behavior suggests constraints due to the rigidity of the tetrahedral group, that are further enhanced at high symmetry.

### INTRODUCTION AND PREVIOUS WORK

Britholite, a rare-earth (REE) mineral isostructural with apatite, has the general formula  $(\text{Na,Ca,REE})_{10}(\text{Si,P})_6\text{O}_{24}(\text{OH,F})_2$  with  $\text{Si} > \text{P}$ . It is one of the most abundant REE-bearing mineral phases, and it is typically found in nepheline syenites and in contact metasomatic rocks related to alkali syenites and granites. Two natural end-members are known, britholite-(Ce) (formerly lessingite) and britholite-(Y) (formerly abukumalite).

Britholite-(Ce) was first described by Winther (1901) as an orthorhombic mineral, pseudo-hexagonal by twinning on (110). Later X-ray work (Hägele and Machatschki 1939) on the same sample gave a hexagonal unit cell ( $a = 9.61$ ,  $c = 7.02\text{ \AA}$ ) and pointed to strong similarities with the apatite-group minerals. Gay (1957) studied three samples of britholite-(Ce), (of which one had significant Na at the REE sites, and another some <sup>141</sup>Zr), and reported hexagonal symmetry, space group  $P6_3/m$ , on the basis of Laue photographs and piezoelectric tests. He also noted biaxial optical behavior in all the crystals; this is incompatible with hex-

agonal symmetry. Hughson and Sen Gupta (1964) described a Th- and Si-rich apatite from the Nb ore-deposit at Oka (Quebec) with hexagonal symmetry ( $a = 9.48$ ,  $c = 6.96\text{ \AA}$ ) and composition  $(\text{Na}_{0.09}\text{Ca}_{6.54}\text{Mg}_{0.06}\text{Fe}_{0.02}\text{Ce}_{1.13}\text{Nd}_{0.61}\text{La}_{0.44}\text{Pr}_{0.14}\text{Sm}_{0.11}\text{Gd}_{0.06}\text{Y}_{0.04}\text{Dy}_{0.01}\text{Th}_{0.28})(\text{P}_{3.08}\text{Si}_{2.63}\text{Al}_{1.12}\text{Ti}_{0.01})\text{O}_{24}(\text{OH}_{0.79}\text{F}_{1.42})$ . This was later recognized to be a mixture of britholite and REE-bearing apatite (Fleet and Pan 1995a). A Th-rich britholite-(Ce) from Monte Somma (Italy) was reported to have composition:  $\text{Ca}_4(\text{Ca}_{1.54}\text{Ce}_{1.77}\text{La}_{0.70}\text{Nd}_{0.47}\text{Pr}_{0.16}\text{Th}_{1.23}\text{U}_{0.08})_{5.95}(\text{Si}_{5.42}\text{P}_{0.94})_{6.36}\text{O}_{26}$ , unit-cell dimensions  $a = 9.597$  and  $c = 7.04\text{ \AA}$ , hexagonal symmetry (from Laue photographs), and uniaxial optical behavior (Orlandi et al. 1989).

Structure refinements in the monoclinic  $P2_1$  space-group were given by De-yu et al. (1981) for britholite-(Ce) ( $a = 9.6283$ ,  $b = 9.6305$ ,  $c = 7.0495\text{ \AA}$ , and  $\gamma = 120.02^\circ$ ) and by Jianhong et al. (1992) for britholite-(Y) [ $(\text{Y}_{5.64}\text{Ca}_{3.16}\text{Ce}_{0.54}\text{Dy}_{0.42}\text{Er}_{0.22})(\text{Si}_{5.90}\text{P}_{0.10})\text{O}_{24}(\text{OH,F})_2$ ;  $a = 9.504$ ,  $b = 9.414$ ,  $c = 6.922\text{ \AA}$ , and  $\gamma = 119.71^\circ$ ;  $R_{\text{obs}} = 11\%$ ]. Accurate structure refinements ( $R_{\text{obs}} = 3\text{--}4\%$ ) of three britholite-(Ce) samples with different compositions [ $(\text{Ca}_{3.21}\text{Na}_{0.90}\text{La}_{1.66}\text{Ce}_{2.71}\text{Pr}_{0.22}\text{Nd}_{0.67})_{5.97}(\text{Si}_{4.29}\text{P}_{1.71})\text{O}_{24}(\text{OH,F})_2$ ,  $(\text{Ca}_{3.45}\text{Na}_{0.0}\text{La}_{2.58}\text{Ce}_{2.80}\text{Pr}_{0.15}\text{Nd}_{0.34})_{5.932}(\text{Si}_{5.78}\text{P}_{0.22})\text{O}_{24}(\text{OH,F})_2$ , and  $(\text{Ca}_{1.40}\text{Na}_{0.97}\text{La}_{2.20}\text{Ce}_{3.69}\text{Pr}_{0.32}\text{Nd}_{0.80})_{5.938}(\text{Si}_{5.69}\text{P}_{0.31})\text{O}_{24}(\text{OH,F})_2$ ]

\* E-mail: oberti@crystal.unipv.it

were provided only recently by Kalsbeek et al. (1990). These authors derived  $P6_3$  symmetry for all the samples studied, discussed the geometries of the three independent REE sites ( $^{19}\text{REE1}$ ,  $^{19}\text{REE1a}$ , and  $^{17}\text{REE2}$ ), and proposed two sequences for REE site-preference, i.e.,  $\text{REE2} \cong \text{REE1} > \text{REE1a}$  for the P-rich sample, and  $\text{REE2} > \text{REE1} \cong \text{REE1a}$  for the other samples; they also noted biaxial optical behavior. Genkina et al. (1991) reported a structure refinement in  $P6_3/m$  ( $R_{\text{obs}} = 5.4\%$ ) of a Sr-rich britholite-(Ce) from the Khibiny alkaline massif (Kola peninsula)  $[(\text{Ca}_{1.40}\text{Sr}_{1.00}\text{Ce}_{1.60}) (\text{Ca}_{0.84}\text{Ce}_{5.16}) \text{Si}_6\text{O}_{24} (\text{O}, \text{OH}, \text{F})_2]$ . They found Sr ordered at the larger ninefold coordinated site, in contrast with the results of Hughes et al. (1991a) who found that Mn is ordered at Ca1 and Sr at Ca2 in apatite. Hughes et al. (1992) refined the structure of Na-bearing britholite-(La) and britholite-(Gd), synthesized by Ito (1968), and found a pseudo-hexagonal  $P2_1$  sub-symmetry of the  $P6_3/m$  apatite atomic arrangement, with the only deviation from hexagonal symmetry being the coordinates of the oxygen atoms. The compositions derived from this refinement were different from those expected [i.e.,  $(\text{Na}_{1.45}\text{La}_{8.55})\text{Si}_6\text{O}_{24}(\text{F}_{0.9}\text{O}_{1.1})$  and  $(\text{Na}_{1.19}\text{Gd}_{8.81})\text{Si}_6\text{O}_{24}(\text{F}_{0.38}\text{O}_{1.62})$ ], suggesting the existence of oxy-britholite. The REE site-preference was  $\text{REE2a} = \text{REE2b} = \text{REE2c} > \text{REE1b} > \text{REE1a}$  for both samples.

Noe et al. (1993) provided accurate structure refinements ( $R_{\text{obs}} = 1.5\text{--}3.5\%$ ) of monoclinic  $P2_1$  metamict britholite-(Ce)  $[(\text{Ca}_{4.48}\text{La}_{0.34}\text{Ce}_{2.46}\text{Pr}_{0.34}\text{Nd}_{0.70}\text{Sm}_{0.08}\text{Eu}_{0.02}\text{Gd}_{0.30}\text{Dy}_{0.14}\text{Ho}_{0.10}\text{Er}_{0.08}\text{Y}_{1.38})\Sigma_{10.42}\text{Si}_{5.58}\text{O}_{24}(\text{OH}_{0.32}\text{F}_{1.68})]$  and britholite-(Y)  $[(\text{Ca}_{2.48}\text{Fe}_{0.42}\text{Mn}_{0.98}\text{La}_{0.02}\text{Ce}_{0.18}\text{Pr}_{0.02}\text{Nd}_{0.20}\text{Sm}_{0.10}\text{Tb}_{0.02}\text{Dy}_{0.52}\text{Ho}_{0.18}\text{Er}_{0.24}\text{Y}_{4.54})\Sigma_{9.90}(\text{Si}_{5.86}\text{P}_{0.26})\text{O}_{24}(\text{OH}_{0.14}\text{F}_{1.86})]$  before and after annealing. The REE site-preference is  $\text{REE2a} = \text{REE2b} = \text{REE2c} > \text{REE1a,b}$ . However, different (inconsistent) total numbers of electrons at the REE sites were obtained before and after annealing. Inspection of the reported data suggests that the refinements of the annealed samples are most reliable; notably, they are very close to hexagonal symmetry.

Thus, some questions are still open in britholite crystal-chemistry: (1) whether previous work had neglected monoclinic symmetry; (2) if not, whether the presence of different symmetries can be related to chemical variations and/or REE distributions (i.e., degrees of order); (3) whether the reported cation vacancies are real or are an artifact due to incomplete analysis; (4) whether column anions affect cation distributions, in analogy to what is observed in apatite (Fleet and Pan 1997).

We report here high-quality ( $R_{\text{obs}} = 1.3\text{--}2.6\%$ ) structure refinements and electron and ion microprobe data of two britholite-(Ce) samples; the first (hereafter called CAPR) is far richer in Th and U (summing to 0.84 atoms per formula unit, apfu) than all previously refined samples. The second (hereafter called LOS) is similar in composition to one of the  $P6_3$  samples of Kalsbeek et al. (1990). A comparison with all literature data on REE-bearing apatites and britholites is also provided.

## EXPERIMENTAL METHODS

### Sample description

Crystal CAPR was manually extracted from a volcanic ejectum collected within a pyroclastic flow unit of the Vico volcanic complex near Capranica, north of Rome (Latium, Italy).

The host-rock can be classified as a silica-saturated alkali-syenite, and contains miarolitic cavities and voids enriched in late-crystallizing minerals such as vonsenite, helvite, baddeleyite, and vicanite. Britholite-(Ce) occurs in these vugs as euhedral, pale greenish-blue prismatic hexagonal crystals up to 1 mm in length. It is associated with hellandite and other REE- and actinide-bearing minerals in late-stage fractures and veins cutting the ejectum (Della Ventura et al. 1999).

Crystal LOS was found in specimen N. 130.61 of the mineralogical collection of the Laboratoire de Minéralogie of the Museum National d'Histoire Naturelle of Paris. It occurs as rare orange-pink hexagonal prisms of 1 mm in length in a miarolitic cavity of an apatitic nepheline-syenite rock (Lacroix 1911; Moreau et al. 1996) from the Rouma Island (Los Islands, Republic of Guinea). Associated minerals in the vug are: Mn-rich aegirine, Mn-rich arfvedsonite, Mn-rich astrophyllite, catapleite, eudyalite, serandite, villiaumite and a REE-Th bearing mineral belonging to the stillwellite group, which is still unidentified.

### X-ray data collection, space group determination, and structure refinement

Crystals were selected on the basis of optical behavior and freedom from inclusions. They were mounted on a Philips PW-1100 automated four-circle diffractometer and examined with graphite monochromatized  $\text{MoK}\alpha$  radiation. Unit-cell dimensions were calculated from least-squares refinement of the  $d$  values obtained from 60 rows of the reciprocal lattice by measuring the center of gravity of each reflection and of its corresponding antireflection in the  $\theta$  range between  $-35$  and  $35^\circ$ . A hemisphere of data  $(hkl, \bar{h}kl, h\bar{k}l, \bar{h}\bar{k}l)$  was collected in order to allow refinement in any Laue group, and the step-scan profile technique of Lehman and Larsen (1974) was used for collection and integration of the diffraction effects. Intensities were then corrected for absorption following the method of North et al. (1968), corrected for Lorentz and polarization effects, averaged and reduced to structure factors.

Anisotropic structure refinements were done on reflections with  $I > 3\sigma(I)$ . Fully ionized scattering factors (with terms for anomalous dispersion) were used for all cationic and anionic sites in which isomorphous substitutions could be present (i.e., Si, REE, and O4), and should be evaluated also from the refined site-scattering (ss); neutral scattering factors were refined against the ionized ones for the remaining oxygen atoms, thus providing estimates for their formal charges. More detail on the refinement procedure is given in Hawthorne et al. (1995). Due to the close atomic numbers of (minor) P and Si, the refined site-scatterings at the Si site were not considered reliable, and scattering curves for  $\text{Si}^0$  vs.  $\text{Si}^{4+}$  were used in the last cycles of the refinements.

Two crystals of britholite-(Ce) from Capranica gave equivalent results as far as both symmetry and structural parameters are concerned. We report here on the crystal for which complete chemical characterization could also be obtained. Due to the poor quality of the crystals, only one refinement could be obtained for sample LOS.

Refinement of the unit-cell parameters was first carried out without restraints, and resulted in deviations lower than  $1\sigma$  from

the ideal hexagonal setting ( $a = b$ ,  $\alpha = \beta = 90^\circ$ ,  $\gamma = 120^\circ$ ). Table 1 reports unit-cell parameters obtained with restraints. The  $N_z$  test done after merging equivalent reflections gave rather ambiguous results, approaching centrosymmetric distribution at low and high  $Z$  values and acentric distribution at intermediate  $Z$  values. This behavior is different from that reported by previous authors (Hughes et al. 1992; Noe et al. 1993), and is also inconsistent with the  $P6_3$  space-group. A reasonable explanation is that REEs occur at the same special positions in both the  $P6_3$  and  $P6_3/m$  space groups, and thus do not allow distinction; their contribution to the  $F_{\text{obs}}$  values prevails over that of the lighter elements occurring at the other sites that obey  $P6_3$  symmetry. Refinement in the  $P6_3$  space-group gave significant deviations from the centrosymmetric arrangement for the Si and O sites, which can be straightforwardly detected from Tables 2 and 3.

The lowering of symmetry from  $P6_3/m$  to  $P6_3$  makes the O3 atom degenerate into O3 and O3a. We compared the difference in their atomic coordinates, and calculated that in  $P6_3$  britholite the tetrahedron is rotated  $\sim 4^\circ$  (sample CAPR) around the Si-O1 bond with respect to  $P6_3/m$  apatite. As a consequence, the O3a atom moves closer to the REE1a site, and the O3 atom moves farther from the REE1 site and closer to the REE2 site (REE2-O3 = 3.18 Å in CAPR, 3.15 Å in LOS), which assumes a [7+1] coordination. The assignment of the O3 atom to the coordination sphere around REE2 is supported by bond-valence calculations. In sample CAPR, we calculated an REE2-O3

bond-valence of  $\sim 0.06$  v.u., similar to the 0.08 v.u. provided by each of the three long REE1-O3 bonds.

Structure refinements in the monoclinic  $P2_1$  space-group were also attempted for both samples. They gave absolutely equivalent results for the sets of sites no longer equivalent in the  $P2_1$  space-group (Si and REE2). However, they were less satisfactory from the point of view of the refinement parameters and of the crystal-chemical interpretation. Details are reported in the Appendix, and a discussion of the different refined models is given in the following section.

Unit-cell and selected refinement parameters are given in Table 1 for the two samples. Atomic coordinates, equivalent isotropic atomic displacement factors (adp), and refined site scatterings (ss) are given in Table 2. Selected interatomic distances are in Table 3. Tables 4 and 5<sup>1</sup> provide observed and calculated structure factors and the anisotropic components of the adps.

### Electron microprobe (EMP) and secondary ion mass-spectrometry (SIMS) analyses

The crystals used for the structure refinement were subsequently mounted in epoxy resin, polished and analyzed both with electron and ion microprobes.

EMP analyses (wavelength dispersion) were done at 15 kV and 20 nA with an ARL instrument using natural mineral standards for calibration. Data were processed with the program PROBE 5.2 (Donovan and Rivers 1990), after Phi-Rho-Z correction following Armstrong (1988).

SIMS analyses were done to quantify all the possible chemical constituents: H, Li, B, Be, F, Ba, Y, La, Ce, Pr, Nd, Sm, Eu, Gd, Dy, Er, Yb, Th, and U. A new procedure based on "energy-filtering" and off line mathematical corrections, was specifically developed to mostly eliminate interferences in the mass

TABLE 1. Selected crystal and refinement data

	CAPR	LOS
$a = b$ (Å)	9.547 (4)	9.682(30)
$c$ (Å)	6.991 (1)	7.066(24)
$V$ (Å <sup>3</sup> )	551.83	573.63
Space group	$P6_3$	$P6_3$
$\theta$ range (°)	2-35	2-35
$hkl$ range	$\pm h, k, \pm l$	$\pm h, k, \pm l$
no. all	873	606
no. obs	648	552
$R$ sym%	4.4	5.4
$R$ all%	2.5	3.1
$R$ obs%	1.3	2.6

TABLE 2. Atomic fractional coordinates, equivalent isotropic atomic displacement parameters, and refined site scatterings (ss; epfu) for the REE sites and refined formal charges (fc, per site) for the anionic sites; first line: CAPR; second line: LOS. The  $z$  coordinate of REE2 was set at 1/4 to fix the origin

Site	mult.	ss, fc	$x/a$	$y/b$	$z/c$	$B_{\text{eq}}^*$
Si1	6	n.r.	0.3990(1)	0.3718(1)	0.2513(9)	0.68
	6	n.r.	0.4007(2)	0.3728(2)	0.2564(10)	1.74
REE1	2	77.5	1/3	2/3	-0.0048(4)	0.85
	2	76.2	1/3	2/3	-0.0039(6)	1.84
REE1a	2	65.6	2/3	1/3	0.0001(5)	0.82
	2	79.7	2/3	1/3	0.0060(6)	1.98
REE2	6	289.9	0.2378(1)	-0.0116(1)	1/4	0.87
	6	298.6	0.2364(1)	-0.0133(1)	1/4	1.84
O1		-1.58	0.3229(3)	0.4886(3)	0.2532(18)	1.45
		-0.09	0.3246(8)	0.4868(7)	0.2589(22)	2.65
O2		-1.00	0.5940(3)	0.4695(3)	0.2569(23)	1.78
		-0.22	0.5929(7)	0.4693(7)	0.2439(32)	3.01
O3		-3.00	0.3168(6)	0.2431(5)	0.4218(7)	2.11
		-0.99	0.3120(12)	0.2445(12)	0.4174(16)	3.48
O3a		-0.35	0.3580(5)	0.2604(5)	0.0595(6)	1.35
		-0.02	0.3650(9)	0.2650(10)	0.0633(13)	2.26
O4	2	17.5	0	0	0.2359(46)	5.38
	2	17.6	0	0	0.1771(40)	8.39

\*  $B_{\text{eq}}$  is calculated from refined anisotropic parameters.

<sup>1</sup>For copies of Tables 4–5, Document AM-01-068, contact the Business Office of the Mineralogical Society of America (see inside cover of a recent issue for price information). Deposit items may also be available on the American Mineralogist web site at <http://www.minsocam.org>.

**TABLE 3.** Selected interatomic distance (Å) and geometrical descriptors

		CAPR	LOS
REE1-O1	×3	2.446(9)	2.518(6)
-O2	×3	2.419(11)	2.522(6)
-O3	×3	3.047(5)	3.144(10)
<REE1-O>		2.637	2.728
V(Å <sup>3</sup> )		34.25	37.92
REE1a-O1	×3	2.389(10)	2.438(6)
-O2	×3	2.510(12)	2.415(6)
-O3a	×3	2.700(40)	2.683(8)
<REE1a-O>		2.533	2.524
V(Å <sup>3</sup> )		31.44	31.31
REE2-O1		2.694(3)	2.727(9)
-O2		2.422(3)	2.469(8)
-O3		2.468(4)	2.518(6)
-O3		2.377(5)	2.417(8)
-O3		3.180(5)	3.148(10)
-O3a		2.618(4)	2.682(7)
-O3a		2.362(4)	2.432(7)
-O4		2.330(2)	2.412(7)
7-<REE2-O>		2.467	2.523
8-<REE2-O>		2.556	2.601
V(Å <sup>3</sup> )		22.21	23.33
Si-O1		1.607(3)	1.604(8)
-O2		1.613(3)	1.614(8)
-O3		1.607(6)	1.584(12)
-O3a		1.632(7)	1.646(11)
<Si-O>		1.615	1.612
V(Å <sup>3</sup> )		2.14	2.09
TAV*		25.52	69.32
TQE†		1.0065	1.0183

\* TAV = tetrahedral angular variance.

† TQE = tetrahedral quadratic elongation.

spectrum (especially in the middle- and heavy-REE region), and to derive accurate ion yields to be used in the quantification procedures (Ottolini and Oberti 2000).

Li and Be contents are extremely low in both samples (at few parts per million concentration level) and were thus neglected in the calculations. Unit-formulae recalculations done on the basis of 26 (O + F) are given in Table 6. The consistency between the chemical (EMPA and SIMS) results and those of the structure refinement may be evaluated by comparing the refined site-scatterings (in electrons per formula unit, epfu) at the various group-sites with those calculated from Table 6. The very good agreement between the two totally independent approaches (REE: 433.0 vs. 424.1 epfu for CAPR, 454.5 vs. 454.3 epfu for LOS; O4: 17.5 vs. 17.8 epfu for CAPR, 17.6 vs. 17.5 epfu for LOS) is evidence of the high accuracy of the data.

## DISCUSSION

### Space-group symmetry of britholite

In the  $P6_3/m$  apatite structure type there is a single tetrahedral site and two Ca sites (<sup>19</sup>Ca1 and <sup>17</sup>Ca2). In REE-bearing apatites with Si contents up to 0.80 apfu, REEs distribute between the Ca1 and Ca2 sites, the preference for Ca2 decreasing along the 4f transition-metal series and being strongly affected by the nature of the column anion (Hughes et al. 1991a, 1991b; Fleet and Pan 1995a, 1995b, 1997). In britholite, the nearly complete substitution of (the larger) Si<sup>4+</sup> for P<sup>5+</sup> at the tetrahedral site allows the REE<sup>3+</sup> concentration to exceed that of Ca<sup>2+</sup>. The combined chemical substitutions induce a re-arrangement of the structure to  $P6_3$  symmetry, in which the tetrahedral and REE2 sites are still unique, and the REE1 site

**TABLE 6.** The composition of britholite as obtained from combined EMP and SIMS analyses; unit-formula recalculation was done on the basis of 26 (O+F)

oxide wt%	CAPR	LOS	formula unit	CAPR	LOS
SiO <sub>2</sub>	21.10	18.40	Si	5.57	5.07
B <sub>2</sub> O <sub>3</sub>	0.35	0.00	B	0.16	0.00
P <sub>2</sub> O <sub>5</sub>	1.11	3.21	P	0.25	0.75
			ΣSi	5.98	5.82
Na <sub>2</sub> O	0.00	1.83	Na	0.00	0.98
CaO	16.80	6.79	Ca	4.75	2.01
MnO	0.18	0.00	Mn	0.04	0.00
BaO	0.00	0.01	Ba	0.00	0.00
Y <sub>2</sub> O <sub>3</sub>	1.71	0.09	Y	0.24	0.01
La <sub>2</sub> O <sub>3</sub>	11.23	28.57	La	1.09	2.90
Ce <sub>2</sub> O <sub>3</sub>	21.70	32.80	Ce	2.10	3.31
Pr <sub>2</sub> O <sub>3</sub>	2.19	2.40	Pr	0.21	0.2
Nd <sub>2</sub> O <sub>3</sub>	5.92	4.25	Nd	0.56	0.42
Sm <sub>2</sub> O <sub>3</sub>	0.72	0.33	Sm	0.07	0.03
Eu <sub>2</sub> O <sub>3</sub>	0.06	0.03	Eu	0.01	0.00
Gd <sub>2</sub> O <sub>3</sub>	0.50	0.30	Gd	0.04	0.03
Dy <sub>2</sub> O <sub>3</sub>	0.31	0.06	Dy	0.03	0.01
Er <sub>2</sub> O <sub>3</sub>	0.14	0.01	Er	0.01	0.00
Yb <sub>2</sub> O <sub>3</sub>	0.12	0.00	Yb	0.01	0.00
ThO <sub>2</sub>	11.92	0.28	Th	0.72	0.02
UO <sub>2</sub>	2.12	0.00	U	0.12	0.00
F	2.12	1.69	ΣREE1-2	10.00	9.96
H <sub>2</sub> O	0.13	0.29	OH	0.23	0.53
O=F	0.89	0.71	F	1.77	1.47
Total	99.54	100.63	ΣO4	2.00	2.00

degenerates into two independent (REE1 and REE1a) sites that are significantly different in site-scattering and geometry (Tables 2 and 3). Further lowering of the symmetry to  $P2_1$  is related to degeneration of the REE2 site (to REE2a,b,c) and of the tetrahedral site (to Si1,2,3).

Structure refinements in the  $P6_3/m$  space group are clearly inadequate. They result in  $R$  factors much higher than those in the  $P6_3$  space group (3.0 vs. 1.3% for CAPR, 4.0 vs. 2.6 for LOS), and in anomalously high atomic displacement factors for all anionic sites, particularly for O3. Refinements in the  $P2_1$  space-group are inadequate as well, since they result in significantly higher  $R$  factors (1.7% for CAPR and 4.0% for LOS), and unrealistic formal charges at those anionic sites which are no longer equivalent in the monoclinic setting. Moreover, they provide equal (within the esd) refined site-scattering values at the REE2a,b,c sites, and equal (within the esd) refined mean bond-lengths at the Si1,2,3 and REE2a,b,c sites (cf. the Appendix), thus excluding any cation-ordering that could justify the lowering of the britholite symmetry to  $P2_1$ . Sample CAPR is particularly useful in this regard, since ordering of its <sup>14</sup>B content (0.16 apfu; Table 6) would provoke anomalously short <cation-oxygen> distances (the ionic radius of <sup>14</sup>B is 0.11 Å, and that of Si 0.26 Å; Shannon 1976). Notably, the geometries at the Si1,2,3 and at the REE2a,b,c sites were similar, (within esd), also in the previous monoclinic refinements (Hughes et al. 1992; Noe et al. 1993), and did not provide a crystal-chemical reason for lowering the symmetry of the model.

The significance of the changes in the  $R$  factor can be assessed by the test of Hamilton (1965). This test can be correctly applied only to sets of data with equal numbers of parameters (in this case, of reflections) and different numbers of variables. Whereas the comparison between  $P6_3/m$  and  $P6_3$  refinements fulfils these requirements, that between  $P6_3$  and  $P2_1$  does not. In principle, we could apply the  $P6_3$  model to a

data set obtained after averaging only the monoclinic pairs (which gives the same number of parameters, but a lower-quality set of non-independent parameters if the correct symmetry is hexagonal). In this way, the *R* factor increases from 1.3% to 2.1% for CAPR, the change being significant on the basis of the Hamilton test, and the results are absolutely equivalent to those reported in Tables 2 and 3. Therefore, averaging the hexagonal pairs lowers the experimental errors, and does not cancel out any structural information.

Twinning with three monoclinic individuals with equal proportions (which could simulate the  $P6_3$  symmetry) was also taken into account. Difference Fourier maps calculated at convergence did not show any residual indicating twinning. The above results coupled with the principle of parsimony suggest that the  $P6_3$  space group best describes the symmetry of the britholite structure.

### Cation site-preference and crystal-chemistry in britholite

**REE sites.** Comparison of the data for the two samples indicates that Na orders at REE1 in LOS, where a longer <REE1-O> distance is coupled with lower site-scattering. When the contribution due to 0.98 Na pfu is subtracted from the refined site-scattering at REE1, we obtain a mean atomic number of 65.4 for the remaining 1.02 atoms per site, which is consistent with the absence of Ca at REE1. This clear ordering pattern is consistent with the conclusion drawn by Fleet and Pan (1995b) on the basis of bond-valence calculations. The higher site-scattering values and the shorter mean bond-distances refined at the REE2 sites suggest that higher-*Z* elements (with shorter ionic radii) strongly prefer lower coordination numbers.

**Tetrahedral sites.** The  $P^{5+}$  content is very low in CAPR (0.24 apfu) and higher in LOS (0.99 apfu). SIMS analyses of CAPR revealed a minor but significant amount (0.16 apfu) of another tetrahedral cation,  $B^{3+}$ . In sample LOS, the  $B^{3+}$  content is virtually null. The crystal-chemical role of  $^{14}B^{3+}$  is intriguing since it combines a lower formal charge with a shorter ionic radius. Thus the presence of  $^{14}B^{3+}$  should couple with that of tetravalent cations at the REE sites, as is the case of Th in sample CAPR. Other Th-bearing britholites have been reported in the literature. Hughson and Sen Gupta (1964) noted that Th (in some britholites from the former USSR) often, but not always, couples with substitution of  $Al^{3+}$ , presumably in tetrahedral coordination. Orlandi et al. (1989) described a sample from Monte Somma (Italy) with up to 1.31 (U, Th) $^{4+}$  apfu. They could exclude the presence of  $Al^{3+}$ , but admittedly did not check for the presence of  $B^{3+}$ . Therefore,  $^{14}B^{3+}$  could be a more frequent constituent of britholite than has been reported. B-rich and Th-rich britholite-group minerals have also been reported from different deposits in former USSR, under the name melanocerite (Kupriyanova and Sidorenko 1963; Portnov et al. 1969).

### Infrared spectroscopy

The IR spectrum of sample CAPR has been collected in the OH-stretching region on a randomly oriented, doubly polished, single-crystal (thickness 80  $\mu m$ ) using a Nicolet NicPlan microscope equipped with a KBr beam-splitter and an MCT, nitrogen-cooled, detector. The unpolarized-light spectrum shows a well-resolved very broad band centered at 3437  $cm^{-1}$ .

In the britholite structure, the H atom is bonded to the O4 atom, which is coordinated solely to the REE2 site. The low vibrational frequency recorded for the analyzed sample is indicative of a fairly strong H bond, whereas the large width of the absorption band is indicative of a wide variety of OH environments due to local short-range order at both the anion and the REE2 site.

The mineralogical literature does not provide other infrared spectra of britholites, whereas detailed information is provided for apatites with variable OH-F contents at O4 (e.g., Baumer et al. 1985 and references therein). According to these data, apatite shows a two-mode behavior (Della Ventura et al. 1993) with respect to the OH-F substitution. The hydroxy endmembers display a unique sharp band at 3573  $cm^{-1}$  that is replaced by a second absorption at around 3545  $cm^{-1}$  as F replaces OH in apatite. For F contents > 50 mol%, only a rather broad absorption at 3541  $cm^{-1}$  is present in the spectrum, which vanishes for higher F concentrations (Baumer et al. 1985). The anion composition of sample CAPR (Table 6) is  $F_{1.77}OH_{0.23}$ . Therefore, the presence of a single OH band is consistent with the behavior of (OH,F)-apatites. The significantly lower vibrational frequency (3437  $cm^{-1}$  vs. 3541  $cm^{-1}$ ) is in accord with a higher bond-valence contribution to the O4 atom in britholite than in apatite; this, in turn, agrees with the ordering of REE $^{3+}$  cations at the REE2 site substituting for divalent  $Ca^{2+}$ .

The quantitative determination of water (*c*, in wt%) in minerals by IR spectroscopy is based on the Lambert-Beer Law:

$$c = (a_i \cdot 1.8) / (\epsilon_i \cdot D)$$

where  $a_i$  is the integral absorption coefficient, *D* is the density,  $\epsilon_i$  is the matrix specific integral molar absorptivity (in  $L \cdot mol^{-1} \cdot cm^{-2}$ ), and the factor 1.8 results from the conversion of the concentration *c* from  $mol^{-1}$  to wt% (Beran et al. 1993; Libowitzky and Rossman 1997). In practice,  $a_i$  is measured from the IR spectrum (taking into account the sample thickness), but  $\epsilon_i$  must be either calibrated for every mineral family or derived by extrapolated working curves. For britholites, the  $\epsilon_i$  value is not known. However, the water content in sample CAPR has been measured by SIMS ( $H_2O = 0.13$  wt%, Table 6); from the above equation, calibration of the measured IR absorption intensity against *c* gives  $\epsilon_i = 23600 L \cdot mol^{-1} \cdot cm^{-2}$ . This value is in fairly good agreement with the working curve of Libowitzky and Rossman (1997).

### Structural variations in the apatite-britholite join

A comprehensive analysis of the crystal-chemical behavior in the apatite-britholite solid-solution has not been published. Previous studies concentrated on the compositional space close to apatite (e.g., Hughes et al. 1991b; Fleet and Pan 1995a, 1995b; 1997). They showed that REE uptake peaks at Nd (ionic radius = 1.11 Å), that REE are preferentially ordered at the Ca2 site, and that their degree of order (as well as the unit-cell volume and the <Ca1-O> and <Ca2-O> distances) vary in a non-linear way as a function of the number of 4*f* electrons. We compared our data with all the structural data available for the apatite-britholite join (Fleet and Pan 1995a, 1995b, 1997; Genkina et al. 1991; Hughes et al. 1989, 1992; Jianhong et al. 1990; Kalsbeek et al. 1990; Khudolozhikin et al. 1973; Noe et al. 1993; Rakovan and Hughes 2000) to investigate possible

structural constraints to REE uptake. The unit-cell data reported by Khudolozhikin et al. (1973) refer to a series of synthetic fluoroapatites and fluorobritholites with variable amounts of Ca, Sr, Y, La, Nd, Eu, Gd, and Yb. Rakovan and Hughes (2000) provided structure refinement of a fluoroapatite with 1.09 Sr apfu substituting for Ca at the Ca2 site. When structures were reported with monoclinic symmetry, we used the average of the *a* and *b* unit-cell edges and the average of the three <REE2-O> bond distances.

The unit-cell parameters in the apatite-britholite join are expected to be a function of the chemical substitutions at the P, Ca, and O4 sites. Figure 1a–b shows that, although the variation in the reported unit-cell volumes is large (around 20%), there is no clear relation between the unit-cell parameters with either the Ca or the P contents. The aggregate ionic radius (<*r*>, i.e., the weighted mean of the ionic radii of the single cations multiplied by their site occupancies), often proved to be useful to check for crystal-chemical correlations. We calculated <*r*> for synthetic samples assuming that the run products were coherent with the stoichiometry of the starting material. This assumption is apparently correct judging from the regular trends observed in Figures 1 and 2. When the available formulae were not stoichiometric, the calculated <*r*> values were normalized to the overall occupancy at the relevant sites.

Figure 2a–d shows that there is no relation between the unit-cell parameters and <*r*> at the tetrahedral site (<*r*<sub>T</sub>>), whereas a marked sigmoidal behavior can be observed as a function of <*r*> at all the three REE sites (<*r*<sup>REE</sup>>). It is evident from Figure 2a,c that the unit-cell edges are not affected by substitutions at the REE sites that give <*r*<sup>REE</sup>> shorter than that of Ca (1.12 Å). On the other hand, they suddenly and strongly increase for <*r*<sup>REE</sup>> values in the range 1.12–1.14 Å. For <*r*<sup>REE</sup>> values > 1.14 Å no further variation is observed. A behavior such that of Figure 2a,c might be consistent with a phase transition and a change of symmetry. On the contrary, *P*6<sub>3</sub>/*m* apatites distribute in the <*r*<sup>REE</sup>> range 1.12–1.24 Å (1.24 Å is the value calculated for sample La<sub>2</sub>Sr<sub>8</sub>Si<sub>2</sub>P<sub>4</sub>F<sub>2</sub> in Khudolozhikin et al. 1973), and *P*6<sub>3</sub> britholites in the range 1.03–1.22 Å (1.22 Å is the value calculated for sample La<sub>4</sub>Sr<sub>6</sub>Si<sub>4</sub>P<sub>2</sub>F<sub>2</sub>). An increase in Sr relative to La implies a corresponding increase of P, with ideal volume variations of +0.44 Å<sup>3</sup> and of –0.025 Å<sup>3</sup> at the involved REE and tetrahedral sites (per 1 apfu exchange). Notably, the strontian fluoroapatite of Rakovan and Hughes (2000) falls at 1.13 Å and is within the trend of the other samples. Figure 2d shows that there are no restrictions to the unit-cell volume in stoichiometric britholites, whereas they are constrained to smaller values in nearly stoichiometric apatites. Thus the behavior in Figure 2c may derive from the intrinsic

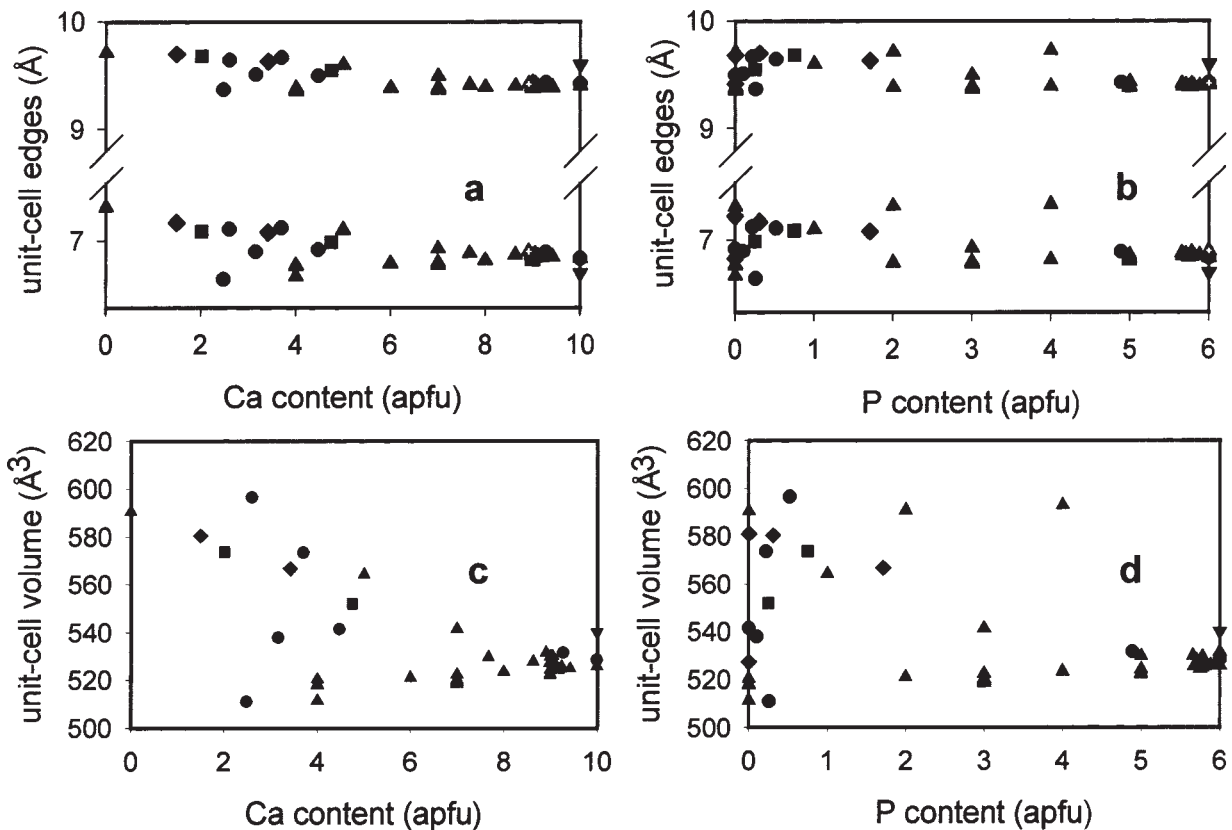


FIGURE 1. The behavior of unit-cell parameters as a function of Ca and P contents (in apfu). ■ = the samples of this work; ▲ = fluoroapatites and britholites (Hughes et al. 1989; 1991; Genkina et al. 1990; Khudolozhikin et al. 1973; Fleet and Pan 1995b, 1997; crossed ▲ = strontian fluoroapatite (Rakovan and Hughes 2000); ▼ = chloro-apatite (Hughes et al. 1989); ◆ = Na-rich apatites and britholites (Hughes et al. 1992; ● = other samples (Hughes et al. 1989, 1991; Kalsbeek et al. 1990; Noe et al. 1993).

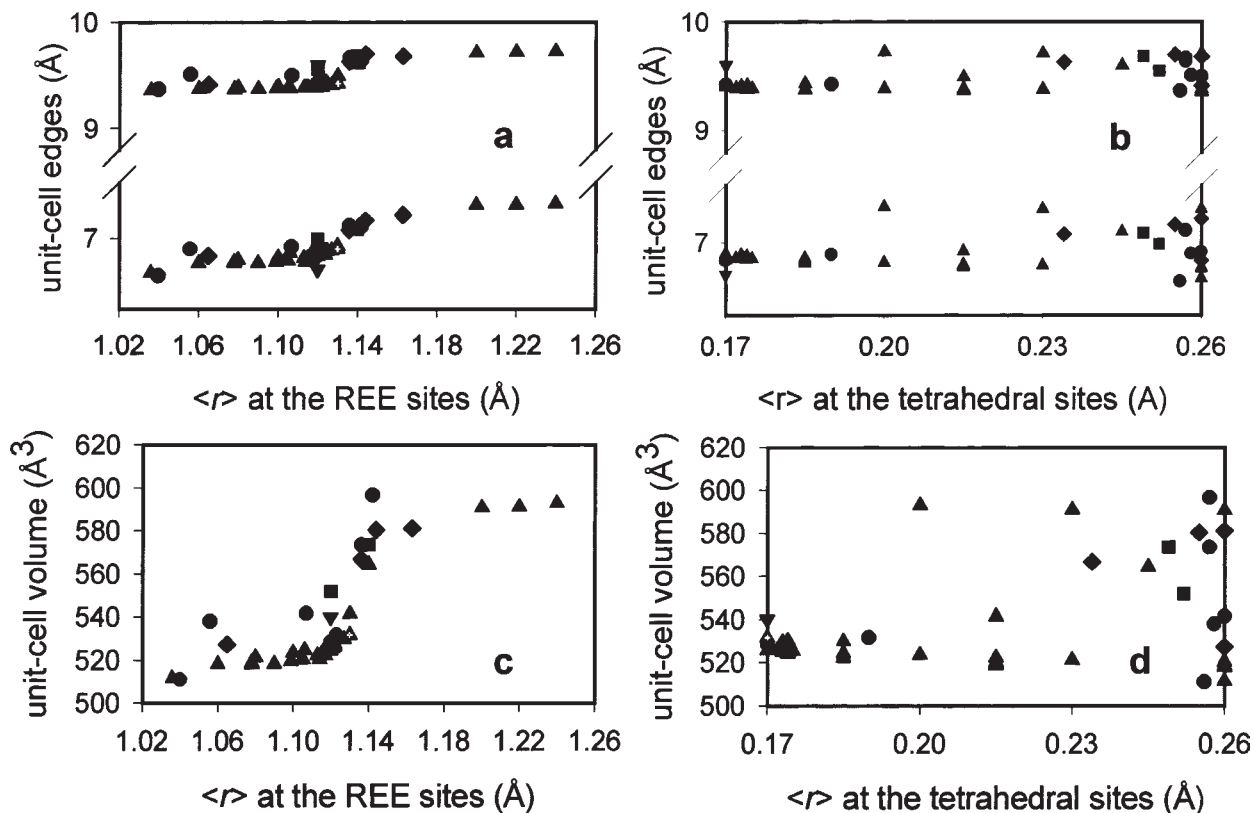


FIGURE 2. The behavior of unit-cell parameters as a function of the calculated aggregate ionic radius ( $\langle r \rangle$ ) at the REE and tetrahedral sites. Same symbols and samples as in Figure 1.

low expandability and the high rigidity of the tetrahedra that connect the REE sites in the apatite structure; it is further increased when the highest symmetry ( $P6_3/m$ ) also prevents rotation around the individual bonds.

Figures 3a and 3b compare the refined grand-mean distances at the tetrahedral and REE sites with the  $\langle r \rangle$  values calculated from the chemical compositions. The “ideal” tetrahedral size is approached only in Na- and Sr-bearing britholites, whereas all other samples plot below the line obtained by summing  $\langle r \rangle$  to 1.38 Å, i.e., the ionic radius tabulated for  $^{14}\text{O}^{2-}$  (this line should be shifted by  $-0.006$  Å in the case of complete F substitution, e.g., for the triangles). Thus the tetrahedra are systematically smaller than expected from  $\langle r \rangle$ , and their constraint to a regular structural expansion is stronger. On the contrary, the REE sites are larger than expected in britholites containing REEs both smaller and larger than Ca. This is in agreement with their strong distortion and with the [7+1] coordination proposed in this work.

The position of the upward (F) and downward (Cl) triangles in the Figures shows that the effect of the column anion on the unit-cell parameters and on the tetrahedral size is small. The O4 site is coordinated solely to the REE2 site, and thus its occupancy can affect uptake and partitioning of the high-Z short-radius REEs and of the actinides (as already noticed in apatite by Fleet and Pan 1997).

Unit-cell volume,  $\langle r \rangle$ , and  $\langle r^{\text{REE}} \rangle$  in the apatite-britholite join are plotted in Figure 4. With the exception of the three

synthetic (La, Sr) fluoro-samples of Khudolozhkin et al. (1973), they define a surface suggesting geometrical restraints to the stability of the apatite structure. The structure refinement of these or similar Sr-rich samples may shed light onto structural restraints and possible site deformation consequent to the incorporation of large cations resulting in  $\langle r^{\text{REE}} \rangle$  longer than 0.15 Å.

#### REE distributions in apatite and britholite

Fleischer and Altschuler (1969) showed that apatites from mafic, ultramafic, and alkaline igneous rocks have dominant Ce-group compositions, whereas those from granitic rocks and granitic pegmatites have a wide range of compositions (from those enriched in Ce-group to those enriched in M- and H-REE, and maxima at Nd, Gd, Dy, or Yb). Apatites from marine sedimentary environments show Ce depletion and La or Nd dominance. The former was related to oxidation to  $\text{Ce}^{4+}$  in seawater and removal through precipitation in hydrous Mn oxides producing Ce-rich Mn nodules (Fleischer and Altschuler 1986). Marine apatites and phosphorites have higher Y contents than most apatites from igneous and metamorphic rocks, consistent with the marked Y-enrichment noted by Høgdahl (1967) in seawater analyses. Iron-ore apatites are enriched in light lanthanides, and similar to apatite from carbonatites, alkaline ultramafic rocks, and ultramafic rocks. They may also approach the rare earth compositions of kimberlites and syenites.

Average REE analyses of britholites from various petrogenetic environments were reported by Fleischer and Altschuler

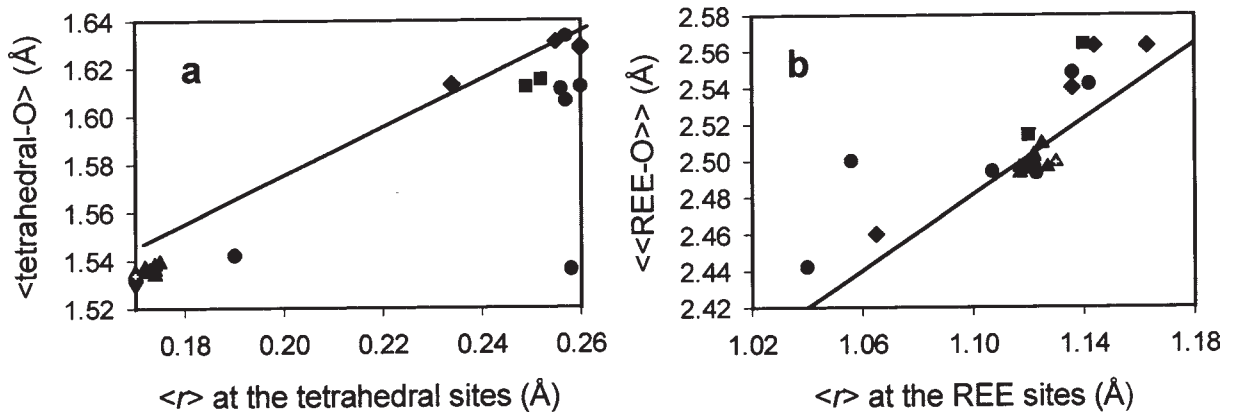


FIGURE 3. Variations in the grand mean of the refined bond distances at the tetrahedral and REE sites (Å) as a function of the aggregate ionic radius calculated from chemical analyses. The lines represent the expected behavior for ionic bonding ( $\langle \text{cat-O} \rangle = \langle r \rangle + 1.38 \text{ \AA}$ ). Same symbols as in Figure 2.

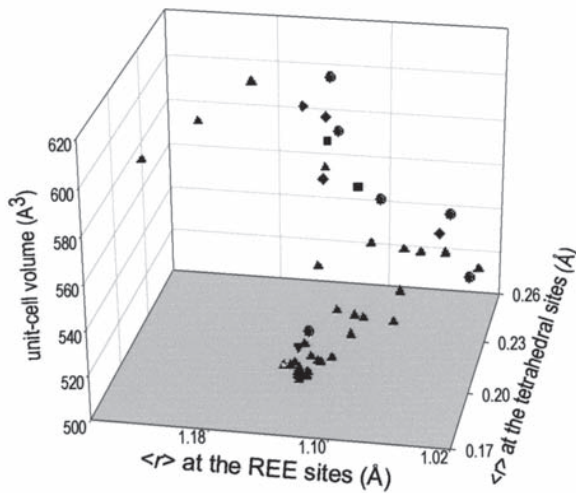
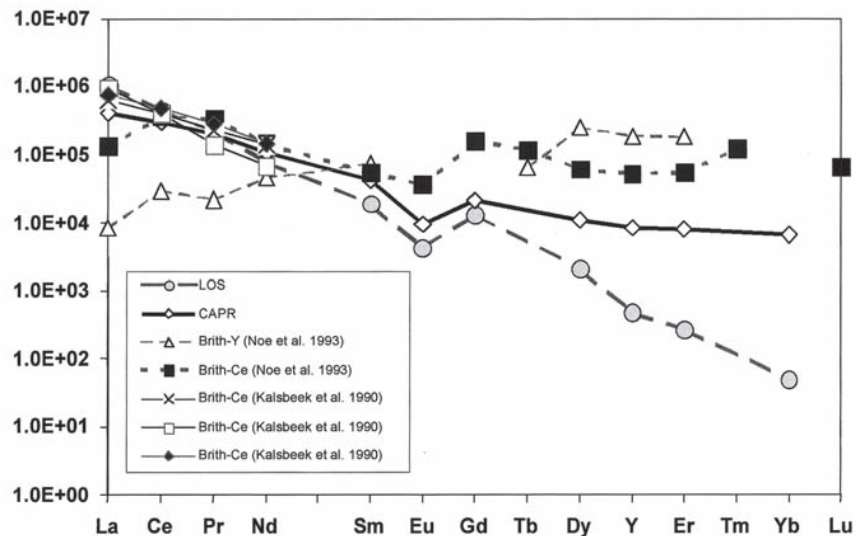


FIGURE 4. Comparison of all the available structural and compositional data suggesting the existence of structural constraints onto chemical variation in the apatite-britholite join.

(1986). The highest  $\Sigma \text{REE}_{\text{ox}}$  values are found in alkalic rocks (~53 wt%), and the lowest in carbonatites (33.4 wt%); alkalic pegmatites have  $\Sigma \text{REE}_{\text{ox}}$  values ~43 wt%. Britholite-(Ce) samples from alkalic rocks and alkalic pegmatites have the highest LREE, whereas britholite-(Y) samples from granitic pegmatites have the highest HREE concentrations.

Figure 5 compares REE patterns of the refined britholite samples (this work; Kalsbeek et al. 1990; Noe et al. 1993), normalized to C1-chondrite values (Anders and Ebihara 1982). In the britholite-(Ce) sample from Los Island, REE are strongly fractionated, with a LREE/HREE ratio of ~10 000. LREE enrichment is less pronounced in the britholite-(Ce) from Capranica. Both samples are characterized by a negative Eu anomaly ( $\text{Eu}/\text{Eu}^* = 0.27$  and  $0.32$  for LOS and CAPR, respectively). Notably, a  $\text{Eu}/\text{Eu}^*$  value of  $0.37$  was found in hellandite-(Ce) coexisting with sample CAPR (Oberti et al. 1999). The patterns of britholite-(Y) and britholite-(Ce) reported by Noe et al. (1993) are different from those of this work, the former having lower LREE and higher HREE contents, and the latter higher Y and HREE contents, and comparable LREE contents (except for La, which is lower). The LREE contents available

FIGURE 5. Chondritic REE patterns for the britholite samples of this work and for those reported in the literature.



for the three britholite-(Ce) samples reported in Kalsbeek et al. (1990) are similar to those of samples LOS and CAPR.

Rakovan and Reeder (1994) showed that uptake and macroscopic distribution of trace elements in apatite may vary during crystal-growth, and identified structurally distinct growth steps on {100}. The step-specific incorporation indicates a mechanistic and non-equilibrium control on partitioning, and explains the different effective distribution coefficients in different regions of the crystal surface. Rakovan and Reeder (1996) analyzed numerous apatites from pegmatites and hydrothermal ore deposits, and showed that such surface growth features are widespread. The surface structural control on REE uptake is very likely to occur also in britholite.

### ACKNOWLEDGMENTS

Enrico Caprilli kindly provided the sample from Latium. Fiorenzo Mazzi provided precious advice in the evaluation of the models refined under different space-group symmetries. Annibale Mottana allowed the use of the IR facilities at the University of Roma Tre. John Rakovan carefully reviewed the manuscript, and significantly improved its readability. Financial support was provided by the Consiglio Nazionale delle Ricerche to the EMP and SIMS laboratories at the Università di Modena and at the CSCC. Financial support to GDV was provided by the Accademia dei Lincei, Commissione per i Musei Naturalistici e Musei della Scienza, and by MURST 1999 "Cristallochimica delle specie minerali: uso di tecniche avanzate per una moderna sistematica."

### REFERENCES CITED

- Anders, E. and Ebihara, M. (1982) Solar-system abundances of the elements. *Geochimica and Cosmochimica Acta*, 46, 2263–2380.
- Armstrong, J.T. (1988) Quantitative analysis of silicate and oxide minerals. Comparison of Monte-Carlo, ZAF and Phi-Rho-Z procedures. *Microbeam Analysis*, 23, 239–246.
- Baumer, A., Ganteaume, M., and Klee, W.E. (1985) Determination of OH ions in hydroxylfluorapatite by infrared spectroscopy. *Bulletin de Minéralogie*, 108, 145–152.
- Beran, A., Langer, K., and Andrut, M. (1993) Single crystal infrared spectra in the range of OH fundamentals of paragenetic garnet, omphacite and kyanite in an eclogitic mantle xenolith. *Mineralogy and Petrology*, 48, 257–268.
- Della Ventura, G., Robert, J.-L., Bény, J.-M., Raudsepp, M., and Hawthorne, F.C. (1993) The OH-F substitution in Ti-rich potassium-richites: Rietveld structure refinement and FTIR and microRaman spectroscopic studies of synthetic amphiboles in the system  $K_2O$ - $Na_2O$ - $CaO$ - $MgO$ - $SiO_2$ - $TiO_2$ - $H_2O$ -HF. *American Mineralogist*, 78, 980–987.
- Della Ventura, G., Williams, C.T., Cabella, R., Oberti, R., Caprilli, E., and Bellatreccia, F. (1999) Britholite-hellandite intergrowths and associated REE minerals from the alkali-syenitic ejecta of the Vico volcanic complex (Latium, Italy): petrological implications bearing on REE mobility in volcanic systems. *European Journal of Mineralogy*, 11, 843–855.
- De-yu, L., Pei-ling, W., and Jian-chen, L. (1981) The crystal-structure of lessingite, rich in light rare earth, cerium. *Acta Crystallographica*, A37, Supplement, C188.
- Donovan, J.J. and Rivers, M.L. (1990) PRSUPR—A PC based automation and analysis software package for wavelength-dispersive electron-beam microanalysis. *Microbeam Analysis*, 25, 66–68.
- Fleet, M.E. and Pan, Y. (1995a) Site preference of rare earth elements in fluoroapatite. *American Mineralogist*, 80, 329–335.
- (1995b) Crystal-chemistry of rare earth elements in fluoroapatite and some calc-silicates. *European Journal of Mineralogy*, 7, 591–605.
- (1997) Site preference of rare earth elements in fluoroapatite: binary (LREE+HREE)-substituted crystals. *American Mineralogist*, 82, 870–877.
- Fleischer, M. and Altschuler, Z.S. (1969) Relationship of the rare-earth composition of minerals to geological environment. *Geochimica and Cosmochimica Acta*, 33, 725–732.
- (1986) The lanthanides and yttrium in minerals of the apatite group—an analysis of the available data. *Neues Jahrbuch Mineralogie Mh.*, 467–480.
- Gay, P. (1957) An X-ray investigation of some rare-earth silicates: cerite, lessingite, beckelite, britholite and stillwellite. *Mineralogical Magazine*, 31, 455–468.
- Genkina, E.A., Malinovskii, Yu.A., and Khomyakov, A.P. (1991) Crystal structure of Sr-containing britholite. *Soviet Physics and Crystallography*, 36, 19–20.
- Hägele, G. and Machatschki, F. (1939) Britholith—ein Cererdesilikatapatit. *Naturwiss.*, 27, 132–133.
- Hamilton, W.C. (1965) Significance tests on the crystallographic R factor. *Acta Crystallographica*, 18, 502–510.
- Hawthorne, F.C., Ungaretti, L., and Oberti, R. (1995) Site populations in minerals: terminology and presentation of results of crystal-structure refinement. *European Journal of Mineralogy*, 33, 907–911.
- Høgdaahl, O. (1967) Distribution of the rare earths in sea-water. *Progress Reports No. 4 to NATO*, Central Institution for Industrial Research, Blindern, Norway, 1–34.
- Hughes, J.M., Cameron, M., and Crowley, K.D. (1989) Structural variations in natural F, OH, and Cl apatites. *American Mineralogist*, 74, 870–876.
- Hughes, J.M., Cameron, M., and Crowley, K.D. (1991a) Ordering of divalent cations in the apatite structure: crystal structure refinement of natural Mn- and Sr-bearing apatite. *American Mineralogist*, 76, 1857–1862.
- Hughes, J.M., Cameron, M., and Mariano, A.N. (1991b) Rare-earth-element ordering and structural variations in natural rare-earth-bearing apatites. *American Mineralogist*, 76, 1165–1173.
- Hughes, J.M., Mariano, A.N., and Drexler, J.W. (1992) Crystal structure of synthetic Na-REE-Si oxyapatites, synthetic monoclinic britholite. *Neues Jahrbuch Mineralogie. Mh.*, 311–319.
- Hughson, M.R. and Sen Gupta, J.G. (1964) A thorium intermediate member of the britholite-apatite series. *American Mineralogist*, 49, 937–951.
- Ito, J. (1968) Silicate apatite and oxyapatites. *American Mineralogist*, 53, 890–907.
- Jianhong, Z., Ze, F., and Libing, L. (1992) A study of crystal structure of britholite-Y. *Acta Mineralogica Sinica*, 12, 131–142.
- Kalsbeek, N., Larsen, S., and Rönso, J.G. (1990) Crystal structure of rare earth elements rich apatite analogues. *Zeitschrift für Kristallographie*, 191, 249–263.
- Khudolozhkin, V.O., Urusov, V.S., and Tobelko, K.I. (1973) Dependence of structural ordering of Rare Earth Atoms in the isomorphous series apatite-britholite (abukumalite) on composition and temperature. *Geochemistry International*, 11, 1171–1177 (translated from *Geokhimiya*, 11, 1595–1602, 1973).
- Kupriyanova, I.I. and Sidorenko, G.A. (1963) Minerals of the britholite group. *Doklady Akademii Nauk SSSR*, 148, 109–111.
- Lacroix, A. (1911) Les syénites nepheliniques de l'archipel de Los e leurs minéraux. *Nouveaux Archives du Muséum Nationale d'Histoire Naturelle*, 3, 1–132.
- Lehman, M.S. and Larsen, F.K. (1974) A method for location of the peaks in step-scan measured Bragg reflection. *Acta Crystallographica*, A30, 580–586.
- Libowitzky, E. and Rossman, G.R. (1997) An IR absorption calibration for water in minerals. *American Mineralogist*, 82, 1111–1115.
- Moreau, C., Ohnestetter, D., Demaiffe, D., and Robineau, B. (1996) The Los Arcipelago nepheline syenite ring-structure: a magmatic marker of the evolution of the central and equatorial Atlantic. *Canadian Mineralogist*, 34, 281–299.
- Noe, D.C., Hughes, J.M., Mariano, A.N., Drexler, J.W., and Kato, A. (1993) The crystal structure of monoclinic britholite-(Ce) and britholite-(Y). *Zeitschrift für Kristallographie*, 206, 233–246.
- North, A.C.T., Phillips, D.C., and Mathews, F.S. (1968) A semi-empirical method of absorption correction. *Acta Crystallographica*, A24, 351–359.
- Oberti, R., Ottolini, L., Cámara, F., and Della Ventura, G. (1999) Crystal structure of non-metamict Th-rich hellandite-(Ce) from Latium (Italy) and crystal chemistry of the hellandite-group minerals. *American Mineralogist*, 84, 913–921.
- Ottolini, L. and Oberti, R. (2000) Accurate quantification of H, Li, Be, B, F, Ba, REE, Y, Th, and U in complex matrices: a combined approach based on SIMS and single-crystal structure refinement. *Analytical Chemistry*, 72, 16, 3731–3738.
- Orlandi, P., Perchiazzi, N., and Mannucci, G. (1989) First occurrence of britholite-(Ce) in Italy (Monte Somma, Vesuvius). *European Journal of Mineralogy*, 1, 723–725.
- Portnov, A.M., Sidorenko, G.A., Dubinchuk, V.T., Kuznetsova, N.N., and Ziborova, T.A. (1969) Melanocerite from the north Baikal region. *Doklady Akademii Nauk SSSR*, 185, 107–109.
- Rakovan, J.F. and Hughes, J.M. (2000) Strontium in the apatite structure: strontian fluorapatite and belovite-(Ce). *Canadian Mineralogist*, 38, 839–845.
- Rakovan, J.F. and Reeder, R.J. (1994) Differential incorporation of trace elements and dissymmetrization in apatite: The role of surface during growth. *American Mineralogist*, 79, 892–903.
- (1996) Intracrystalline rare earth element distributions in apatite: surface structural influences on incorporation during growth. *Geochimica and Cosmochimica Acta*, 60, 4435–4445.
- Shannon, R.D. (1976) Revised effective ionic radii and systematic studies of interatomic distances in halides and chalcogenides. *Acta Crystallographica*, A32, 751–767.
- Winther, C. (1901) Britholith, ein neues mineral. *Zeitschrift für kristallografie und mineralogie*, 34, 685–687.

MANUSCRIPT RECEIVED OCTOBER 20, 2000

MANUSCRIPT ACCEPTED MAY 7, 2001

MANUSCRIPT HANDLED BY JOHN RAKOVAN

**APPENDIX: RELEVANT RESULTS OF THE STRUCTURE REFINEMENT OF BRITHOLITE CAPRANICA IN THE  $P2_1$  SPACE GROUP**

**APPENDIX TABLE 1A.** Atomic fractional coordinates, equivalent isotropic atomic displacement parameters, refined site scatterings (ss; epfu) for the REE sites and refined formal-charges for the anionic sites

	ss, fc	<i>x/a</i>	<i>y/b</i>	<i>z/c</i>	<i>B<sub>eq</sub></i>
Si1	n.r.	0.6282(1)	0.0272(1)	0.2494(8)	0.65
Si2	n.r.	0.3990(1)	0.3717(1)	0.2517(9)	0.72
Si3	n.r.	0.9730(1)	0.6010(1)	0.2560(8)	0.69
REE1a	72.7	0.6662(1)	0.3332(1)	0.0055(1)	0.90
REE1b	70.5	0.6671(1)	0.3334(1)	0.5005(1)	0.78
REE2a	96.8	0.2378(1)	0.9884(1)	0.2500	0.88
REE2b	96.8	0.7506(1)	0.7622(1)	0.2498(3)	0.88
REE2c	96.8	0.0116(1)	0.2495(1)	0.2510(3)	0.88
O1a	-0.78	0.5125(4)	0.8345(4)	0.2420(12)	1.27
O1b	-0.94	0.3223(5)	0.4878(4)	0.2585(21)	1.41
O1c	-1.84	0.1649(4)	0.6772(4)	0.2582(21)	1.43
O2a	-0.82	0.8757(4)	0.4061(4)	0.2629(19)	1.67
O2b	-2.00	0.5945(4)	0.4697(4)	0.2441(21)	1.76
O2c	-0.70	0.5312(5)	0.1245(5)	0.2679(14)	1.58
O3a	-0.02	0.9010(5)	0.6399(5)	0.0636(7)	1.16
O3b	-2.36	0.9282(6)	0.6859(7)	0.4263(8)	1.86
O3c	-1.20	0.3599(5)	0.2601(5)	0.0631(7)	1.21
O3d	-2.00	0.3136(7)	0.2418(6)	0.4266(8)	1.90
O3e	-0.02	0.7387(6)	0.0976(6)	0.0604(8)	1.54
O3f	-3.60	0.7570(5)	0.0748(3)	0.4247(7)	1.95
O4	8.7	0.0004(6)	0.0004(6)	0.2230(16)	4.15

**APPENDIX TABLE 1B.** Selected interatomic distance (Å) and geometrical descriptors

Si1-O1a	1.605(1)	Si2-O1b	1.606(1)	Si3-O1c	1.598(1)
-O2c	1.613(1)	-O2b	1.617(1)	-O2a	1.613(1)
-O3e	1.613(1)	-O3c	1.618(1)	-O3a	1.635(1)
-O3f	1.631(1)	-O3d	1.639(1)	-O3b	1.614(1)
<Si1-O>	1.615	<Si2-O>	1.620	<Si3-O>	1.615
REE1a-O1a	2.477(1)	REE1b-O1a	2.369(1)		
-O1b	2.393(1)	-O1b	2.450(1)		
-O1c	2.400(1)	-O1c	2.448(1)		
-O2a	2.516(1)	-O2a	2.414(1)		
-O2b	2.417(1)	-O2b	2.508(1)		
-O2c	2.535(1)	-O2c	2.391(1)		
-O3a	2.684(1)	-O3b	3.069(2)		
-O3c	2.675(1)	-O3d	3.077(1)		
-O3e 9	2.692(1)	-O3f	3.069(1)		
<REE1a-O>	2.532	9<REE1b-O>	2.641		
		6<REE1b-O>	2.430		
REE2a-O1c	2.692(1)	REE2b-O1a	2.686(1)	REE2c-O1b	2.689(1)
-O2c	2.431(1)	-O2b	2.420(1)	-O2a	2.422(1)
-O3b	3.172(2)	-O3a	2.607(1)	-O3a	2.388(1)
-O3c	2.602(1)	-O3b	2.482(1)	-O3b	2.347(1)
-O3d	2.480(1)	-O3c	2.394(1)	-O3d	3.168(1)
-O3e	2.370(1)	-O3d	2.336(1)	-O3e	2.624(1)
-O3f	2.359(1)	-O3f	3.197(1)	-O3f	2.472(1)
-O4	2.334(1)	-O4	2.338(1)	-O4	2.335(1)
7<REE2a-O>	2.467	7<REE2b-O>	2.466	7<REE2c-O>	2.468
8<REE2a-O>	2.555	8<REE2b-O>	2.557	8<REE2c-O>	2.556